chromocenes, particularly in having much shorter Cr-C(pentadienyl) bond distances than would otherwise be expected and in forming relatively strongly bound 18-electron ligand adducts. The formation of these adducts is additionally unusual in that a concomitant change in pentadienyl coordination from the usual η^5-U form to the unusual η^5-S form results. However, upon oxidation to the 17-electron cations, the pentadienyl ligand reverts back to the usual η^5-U form, demonstrating a narrow window of stability for the η^5-S coordination. Besides the 18-electron mono(ligand) adducts, it is also possible to prepare 18-electron bis(ligand) adducts, in which η^3-pentadienyl coordination is present.

Half-open chromocene carbonyl complexes undergo CO substitution via the same mechanism and at approximately the same rate as their 17-electron vanadium counterparts. Substituents on the pentadienyl ligand may cause steric acceleration of the rate of dissociation, while substituents on the cyclopentadienyl ligand appear to exert electronic influences that result in a retardation in rate. Unusually low, even negative, entropies of activation characterize these reactions and may be attributed to a reorganization of η^5-S to η^5-U pentadienyl coordination. The slow rates of CO addition to these complexes (which require an $\eta^5 \rightarrow \eta^3$ transformation of the pentadienyl ligand) suggest that no ring slippage occurs in the transition state of the CO substitution reactions.

Note Added in Proof. We have learned from Prof. Robert Waymouth of his group's recent syntheses and structural characterizations of $Cp^*(2,4\text{-}C_7H_{11})Cr$ and its monocarbonyl adduct. Both structures are consistent with those found in the present study.

Acknowledgment. F.B. and R.D.E. express their appreciation for generous support of this research by the National Science Foundation and a Faculty Fellow Award from the University of Utah (R.D.E.). We are grateful to R. M. Waymouth for providing details of his unpublished work.

Supplementary Material Available: Listings of IR and mass spectral data, anisotropic thermal parameters, hydrogen atom parameters, least-squares-plane data, positional parameters for non-hydrogen atoms, and bond distances and angles for $Cp(C_5H_7)Cr(CO)_2$ (19 pages); tables of observed and calculated structure factors (14 pages). Ordering information is given on any current masthead page.

Zinc and Magnesium Substitution in Hemoglobin: Cyclic Electron Transfer within Mixed-Metal Hybrids and Crystal Structure of MgHb

Debasish Kuila,[†] Michael J. Natan,[†] Paul Rogers,[‡] David J. Gingrich,[†] Wade W. Baxter,[†] Arthur Arnone,[‡] and Brian M. Hoffman*,[†]

Contribution from the Department of Chemistry, Northwestern University, 2145 Sheridan Road, Evanston, Illinois 60208, and Department of Biochemistry, University of Iowa, Iowa City, Iowa 52242. *Received December 24, 1990*

Abstract: Studies of long-range electron transfer within mixed-metal hemoglobin (Hb) hybrids [α_2(FeP), β_2(MP)] (M = Mg, Zn; P = protoporphyrin IX) are reported, along with the X-ray crystal structure of magnesium-substituted hemoglobin (MgHb). MgHb adopts the quaternary structure of deoxyHb, and replacement of Fe by Mg causes negligible structural changes, supporting earlier inferences that electron transfer (ET) in these hybrids occurs between redox centers held at fixed and crystallographically known distance and orientation. Upon flash photolysis of the [MP, $Fe^{3+}(H_2O)$P] hybrids, the charge-separated intermediate [$(MP)^+$, Fe^{2+}P] (I) is formed by a photoinitiated ^{3}(MP) $\rightarrow$ Fe^{3+}P intramolecular electron-transfer process with rate constant k_i and returns to the ground state by a $Fe^{2+}P \rightarrow (MP)^+$ thermal electron transfer with rate constant k_b. By use of the transient absorption technique, we have measured k_i and k_b for M = Mg and Zn as a function of temperature between 0 and 25 °C. The rate constant, k_i = 35 (8) s^{-1}, for Mg at room temperature is significantly lower than that of Zn, k_i = 85 (15) s^{-1}, although the driving force is greater in the former by about 100 mV. The charge recombination rate, k_b, within [Zn, Fe] is 350 (35) s^{-1} compared to that of 155 (15) s^{-1} for [Mg, Fe]. The inequality, $k_{b,i}^{Zn} \neq k_{b,i}^{Mg}$, rules out rate-limiting conformational "gating" for photoinitiated and thermally activated electron-transfer processes, and further indicates that in both cases ET is direct. Comparisons among the rate constants indicate that the electronic-coupling matrix element between redox sites, $|H_{AB}|^2$, may be slightly (roughly 2-fold) greater for M = Zn than for M = Mg.

Recently it has become possible to study long-range interprotein electron transfer[1] without the complication of second-order processes, through use of modified proteins that hold an electron donor/acceptor redox pair at a fixed distance.[2] In one approach, long-range electron transfer within protein-protein complexes can be accomplished by replacing the heme (FeP) of one protein partner with a closed-shell porphyrin MP[3] (M = Zn, Mg; P = protoporphyrin IX), which permits a photoinitiated ET cycle that begins with the ^{3}(MP) $\rightarrow$ Fe^{3+}P process.[4,5] Mixed-metal [MP, FeP] hemoglobin (Hb) hybrids are particularly suited to the study of long-range electron-transfer processes because replacement of Fe with these closed-shell metal ions causes negligible perturbation of the protein structure. For example, the X-ray crystal structure

[†] Northwestern University.
[‡] University of Iowa.

(1) (a) Gray, H. B.; Malmström, B. G. *Biochemistry* **1989**, *28*, 7499-7505. (b) Marcus, R. A.; Sutin, N. *Biochim. Biophys. Acta* **1985**, *811*, 265-322.

(2) (a) McLendon, G. *Acc. Chem. Res.* **1988**, *21*, 160-167. (b) Cowan, J. A.; Upmacis, R. K.; Beratan, D. N.; Onuchic, J. N.; Gray, H. B. *Ann. N.Y. Acad. Sci.* **1988**, *550*, 68-84. (c) Zang, L.-H.; Maki, A. H. *J. Am. Chem. Soc.* **1990**, *112*, 4346-4351. (d) Therien, M. J.; Selman, M.; Gray, H. B.; Chang, I.-Jy.; Winkler, J. R. *J. Am. Chem. Soc.* **1990**, *112*, 2420-2422. (e) Canters, G. W.; Hali, F. C.; Floris, R.; van de Kamp, M. *J. Am. Chem. Soc.* **1990**, *112*, 907-908.

(3) Abbreviations: hemoglobin, Hb; metalloprotoporphyrin IX, MP; metal-substituted hemoglobin, MHb; mixed-metal hemoglobin hybrids [MP, FeP]; high-performance liquid chromatography, HPLC; isoelectric focusing, IEF; potassium phosphate, KP_i; inositol hexaphosphate, IHP.

0002-7863/91/1513-6520$02.50/0

of MgHb, reported here, is indistinguishable from that of deoxyHb, and under the conditions of our experiments, the hemoglobin tetramers in solution adopt the deoxyHb (T-state) structure. Thus, electron transfer in this system occurs between redox centers held at crystallographically known distance and orientation.

Electron transfer between MP and FeP in a tetrameric $[\alpha_2(Fe^{3+}P), \beta_2(MP)]$ or $[\alpha_2(MP), \beta_2(Fe^{3+}P)]$ Hb hybrid might in principle occur between α_1/β_1 or α_2/β_2 subunits. However, the distance between α_1 and β_1 hemes is over 10 Å greater than the corresponding distance between α_1 and β_2. This additional distance is expected and indeed is found to reduce ET rates by several orders of magnitude.[1,6] Hence, for all practical purposes we may treat the tetramer in terms of two independent $\alpha_1-\beta_2$ electron-transfer complexes. Electron transfer between the MP and FeP groups within such a metal-substituted electron-transfer complex is initiated by photoexcitation of the metal-substituted porphyrin, MP; excitation is to an excited singlet state, but intersystem crossing yields the slowly decaying triplet state, ^{3}(MP). The ^{3}(MP) is a good reductant and can reduce the ferriheme partner ($Fe^{3+}P$) by long-range electron transfer with a photoinitiated electron-transfer rate constant k_l (eq 1). The resulting charge-separated

$$\underset{A^*}{[^3(MP), Fe^{3+}P]} \xrightarrow{k_l} \underset{I}{[(MP)^+, Fe^{2+}P]} \qquad (1)$$

intermediate I returns to the ground state by electron transfer from $Fe^{2+}P$ to the $(MP)^+$ cation radical with rate constant k_b (eq 2).

$$\underset{I}{[(MP)^+, Fe^{2+}P]} \xrightarrow{k_b} \underset{A}{[MP, Fe^{3+}P]} \qquad (2)$$

Triplet-state-quenching studies can be used to probe the photoinitiated process (eq 1), provided that additional energy-transfer quenching processes are not operative, but yield no information about the reaction of eq 2. We now describe in detail the procedures by which the transient absorption technique can be used to measure both k_l and k_b, using the pair of hybrids $[\alpha_2(Fe^{3+}(H_2O)P), \beta_2(MP)]$ (M = Zn, Mg) as the experimental vehicle.

Experimental Section

Materials. Hemoglobin was acquired from a single donor at Evanston Hospital. Rhodamine 6G, $K_3Fe(CN)_6$, and $Na_2S_2O_4$ were obtained from Aldrich. Sephadex G25-150, catalase, glucose oxidase (Type X), glucose, and phytic acid (IHP) were from Sigma Chemical Co. K_2HPO_4 and KH_2PO_4 were from Mallinckrodt. Samples of zinc protoporphyrin (ZnP) and magnesium protoporphyrin (MgP) were obtained from Porphyrin Products or were synthesized according to slight modifications of literature procedures.[7] H_2O was obtained from a MilliQ water purification system. Prepurified N_2 from Matheson was used for all degassing operations, and prepurified CO (99.5%) from Matheson was used.

Protein Preparation. For preparation of hybrids, Hb was split into its component α and β chains by use of a modification of the procedure of Bucci and Fronticelli,[8] followed by heme removal from the β chains as described.[9] Following reconstitution[10] of the β chains with MP (M = Zn, Mg), the β(MP) chains and α(Fe(CO)P) chains were mixed to form the hybrid tetramer. Purification of the reconstituted tetrameric [β(MP), α(Fe(CO)P)] hybrid was accomplished by ion-exchange HPLC (Beckman SP-5PW preparative column (21.5 mm)) at 4 °C using a linear 25 mM KP_i/pH 6.0 to 25 mM dibasic KP_i gradient. Analogous procedures provide the [α_2(MP), β_2(Fe(CO)P)] hybrids. Final purity of the hybrids was confirmed by analytical isoelectric focusing (IEF) using precast polyacrylamide gels (Pharmacia/LKB Ampholine Pageplate, pH 5.5–8.5, or Isolab Resolve IEF, pH 6–8). The protein bands were stained with Coomassie Blue and/or Isolab Resolve-Hb heme stain. A fuller description of this procedure will be presented elsewhere.[10] The fully substituted MHb's were prepared directly from apoHb, reconstituted with the respective MP,[10] and purified as for the hybrids. Samples of [MP, Fe^{2+}(CO)P] and MHb were stored as pellets in liquid N_2.

MgHb Crystals and Their X-ray Analysis. MgHb was crystallized from a solution of 2.3 M ammonium sulfate and 0.3 M ammonium phosphate at pH 6.8 according to the procedure published by Perutz.[11] These crystals belong to space group $P2_1$ with an asymmetric unit of a single $\alpha_2\beta_2$ tetramer. X-ray diffraction data were collected to a resolution of 2.1 Å (a total of 26 667 diffraction maxima with intensities greater than 4 times their standard error) with the multiwire area detectors at the UCSD Resource for Protein Crystallography.

The 1.7-Å structure of human deoxyhemoglobin[12] was used as a starting point. While this atomic model had been fully refined by Fermi et al.,[12] we chose to use a different restrained least-squares refinement program, PROLSQ,[13] in this study. Therefore, the human deoxyhemoglobin model was further refined with PROLSQ against the same 1.7-Å data set used by Fermi et al.[12] This "conditioned" model of human deoxyhemoglobin—with Mg^{II} atoms replacing the Fe^{II} atoms—was used as a starting model for MgHb, and it was refined against the 2.1-Å MgHb diffraction data by use of PROLSQ. After 11 refinement cycles, an R value of 0.20 was obtained (for the data between 20 and 2.1 Å) while the atomic model maintained very good stereochemistry (see Table I).

General Procedures. All manipulations involving Zn- or Mg-substituted hemoglobins were carried out in the dark. Oxidation of [MP, Fe^{2+}(CO)P] to [MP, $Fe^{3+}(H_2O)$P] at pH ~ 7 was effected over the

Table I. Summary of Restrained Least-Squares Refinement (Hendrickson, 1985) Parameters for MgHb

parameter	target σ^a	rms Δ^b
bonding distances, Å[c]		
1–2 bond lengths	0.010	0.012
1–3 angle distances	0.015	0.027
1–4 planar distances	0.030	0.042
special distances	0.300	0.159
planar group deviations from plane, Å	0.010	0.011
chiral center vol, Å^3	0.10	0.16
nonbonded contacts, Å		
separated by a single torsion angle	0.20	0.17
all other van der Waals contacts	0.20	0.17
possible hydrogen bonds	0.20	0.17
conformational torsion angles, deg		
planar (peptide ω)	5.0	3.6
staggered (e.g. aliphatic χ)	10.0	22.0
transverse (e.g. aromatic χ_2)	10.0	32.5
deviations from noncrystallographic symmetry		
main-chain positions, Å	0.30	0.11
side-chain positions, Å	0.30	0.23
main-chain temperature factors, Å^2	1.5	1.2
side-chain temperature factors, Å^2	3.0	2.8
isotropic temperature factors, Å^2		
main-chain (1–2 neighbors)	1.5	1.9
main-chain (1–3 neighbors)	2.0	2.6
side-chain (1–2 neighbors)	4.0	6.8
side-chain (1–3 neighbors)	6.0	9.3

[a] Estimated standard deviations, where $1/\sigma^2$ is used as a relative weighting factor in the minimized sum of observational functions. [b] Root-mean-square deviation from ideal values (as determined from accurate small-molecule crystal structures in the case of bonding distances, chiral volumes, and nonbonded contacts) or from average values (in the case of isotropic temperature factors). [c] 1–2 neighbors = covalently bonded atom pairs; 1–3 neighbors = atom pairs separated by two covalent bonds; 1–4 planar neighbors = atom pairs in a planar group separated by three covalent bonds; special distances = 1–2 and 1–3 distances between the heme iron and the proximal histidine.

(4) (a) Natan, M. J.; Hoffman, B. M. *J. Am. Chem. Soc.* **1989**, *111*, 6468–6470. (b) Natan, M. J.; Kuila, D.; Baxter, W. W.; King, B. D.; Hawkridge, F. M.; Hoffman, B. M. *J. Am. Chem. Soc.* **1990**, *112*, 4081–4082. (c) Hoffman, B. M.; Natan, M. J.; Nocek, J. M.; Wallin, S. A. *Struct. Bonding (Berlin)* **1990**, *75*, 1–24.
(5) (a) Nocek, J. M.; Liang, N.; Wallin, S. A.; Mark, A. G.; Hoffman, B. M. *J. Am. Chem. Soc.* **1990**, *112*, 1623–1625. (b) Nocek, J. M.; Stemp, E. D. A.; Finnegan, M. G.; Kosky, T. L.; Johnson, M. K.; Margoliash, E.; Mauk, A. G.; Smith, M.; Hoffman, B. M. *J. Am. Chem. Soc.*, in press.
(6) Gingrich, D. J.; Nocek, J. M.; Natan, M. J.; Hoffman, B. M. *J. Am. Chem. Soc.* **1987**, *109*, 7533–7534.
(7) Adler, A. D.; Longo, F. R.; Kampas, F.; Kim, J. J. *Inorg. Nucl. Chem.* **1970**, *32*, 1443–1445.
(8) Bucci, E.; Fronticelli, C. *J. Biol. Chem.* **1965**, *240*, 551–552.
(9) Scholler, D. M.; Wang, M. R.; Hoffman, B. M. *Methods Enzymol.* **1978**, *53*, 487–493.
(10) Manuscript in preparation.
(11) Perutz, M. F. *J. Cryst. Growth* **1968**, *2*, 54–56.
(12) Fermi, G.; Perutz, M. F.; Shaanan, B.; Fourme, R. *J. Mol. Biol.* **1984**, *175*, 159–174.
(13) Hendrickson, W. A. *Methods Enzymol.* **1985**, *115*, 252–270.
(14) Zemel, H.; Hoffman, B. M. *J. Am. Chem. Soc.* **1981**, *103*, 1192–1201.

Table II. Analytical Optical Data for [α(FeP), β(MP)] Hybrids

species	λ_1, nm	λ_2, nm	$R = A_{\lambda_1}/A_{\lambda_2}$[a]
[ZnP, $Fe^{3+}(H_2O)P$]	406	424	0.63
[ZnP, $Fe^{2+}P$]	406	424	0.31
[MgP, $Fe^{3+}(H_2O)P$]	406	420	0.70
[MgP, $Fe^{2+}P$]	406	420	0.31

[a] For the definition of R, see Experimental Section, eq 3.

course of 2 h with an approximately 5-fold excess of 5 mM $K_3Fe(CN)_6$ at 4 °C under a N_2 purge. The oxidized protein was applied to a column of Sephadex G-25 equilibrated with pH 7.0, 10 mM KP_i for separation from $[Fe(CN)_6]^{3-}$ and $[Fe(CN)_6]^{4-}$. The [α_2(MP), $\beta_2(Fe^{3+}(L)P$] hybrids, where L = H_2O, are not conveniently used for studies of ET because they autoreduce; in other cases (e.g., L = CN^-, imidazole), this is not a problem.[4b,30]

Reduction of [MP, $Fe^{3+}(H_2O)P$] to [MP, $Fe^{2+}P$] was achieved with freshly prepared, anaerobic solutions of $Na_2S_2O_4$ whose concentrations were determined by titration against $K_3Fe(CN)_6$. Usually 1.1–1.2 equiv of $Na_2S_2O_4$ per ferric heme was added to an anaerobic sample of [MP, $Fe^{3+}(H_2O)P$] at 4 °C; reduction was immediate. The [MP, $Fe^{3+}(H_2O)P$] samples were stored as pellets in liquid N_2.

Sample Preparation. Preparation of samples for flash photolysis was performed under a N_2 atmosphere at 4 °C. Typically, a glass or quartz tonometer containing 2 mL of N_2-purged buffer, pH 7, 10 mM KP_i, and 50 μL of 1 mM IHP was subjected to several evacuation/N_2 backfill cycles. Residual traces of O_2 were removed by subsequent addition of 5 μL of 1 M glucose, 5 μL of 10 mg/mL glucose oxidase, and 5 μL of 2.5 mg/mL catalase under a N_2 blanket. Experiments conducted on rigorously degassed samples without these components gave identical results. Finally, 50–100 μL of oxidized hybrid was added under N_2. Optical spectra were recorded before and after Hb hybrid addition and periodically during flash photolysis.

Instrumentation and Data Analysis. Optical spectra were recorded by using an HP 8451A diode array spectrophotometer. A Gilson HPLC instrument was used for protein purification. Elution profiles were monitored by optical absorbance at 420 nm. Isoelectric focusing was performed on an LKB Multiphor II electrophoresis unit.

Actinic sources utilized for these transient absorbance studies included an Electrophonics flash-lamp-pumped dye laser (Rhodamine 6G emission maximum at 590 nm, ≤1-μs flash duration) or a Vivitar or Sunpack camera flash ($^1/_8$ or $^1/_{16}$ power). The analyzing beam employed a W–I_2 lamp (250 W), J-Y H-20 pre- and post-monochromators, and an RCA 1P28 photomultiplier tube. The photomultiplier current was conditioned with a home-built I/V converter–amplifier, and the output voltage was digitized by an Epic Instruments transient digitizer (Wavesaver Model 10v3; 10 MHz, 4096 8-bit channels) operating in pretrigger mode. Digitized transients were transferred to an IBM-compatible computer. Signal averaging was utilized as needed to achieve the desired signal/noise ratio: triplet-decay data typically were averages of 1–5 transients, while kinetic traces for charge-separated intermediates often consisted of ~50 averaged transients. Time-resolved luminescence measurements are described elsewhere.[5] Data were fit with the Marquardt nonlinear least-squares algorithm.[15] All reported electron-transfer rate constants represent the average of several measurements. Samples in quartz or glass tonometers were held in a thermostated holder.

Spectra. The fraction of oxidized Fe-containing chains within a hybrid, g ($0 \le g \le 1$), can be calculated by using eq 3, where $A_{\lambda 1}^{ox}$, $A_{\lambda 2}^{ox}$,

$$g = (A_{\lambda 1}^{red} - RA_{\lambda 2}^{red})/[R(A_{\lambda 2}^{ox} - A_{\lambda 2}^{red}) - (A_{\lambda 1}^{ox} - A_{\lambda 1}^{red})] \quad (3)$$

$A_{\lambda 1}^{red}$, and $A_{\lambda 2}^{red}$ are the absorbances of a fully oxidized and a fully reduced reference sample at the wavelengths λ_1 and λ_2, and $R = A_{\lambda 1}/A_{\lambda 2}$ is the measured absorbance ratio for a sample of unknown g. Values of R for fully oxidized and fully reduced Hb hybrids are given in Table II.

[^{3}(MP)–MP] difference spectra for M = Zn and Mg in the range 380–600 nm were obtained as the wavelength dependence of the zero-time absorbance changes measured upon flash photolysis of MHb. Extinction coefficients for M = Zn are based on the results previously reported;[14] those for M = Mg were obtained by procedures developed previously[14] using a value of ε(415 nm) = 120 000 M^{-1} cm^{-1} per subunit of MgHb.[16]

Extinction coefficient differences, $\Delta\epsilon_{A^*-A} = \epsilon_{A^*}(\lambda) - \epsilon_A(\lambda)$, for both M's are listed in Table III. The {[MP, $Fe^{2+}P$]–[MP, $Fe^{3+}(H_2O)P$]} difference spectrum was generated by digital subtraction of spectra for [MP, $Fe^{3+}(H_2O)P$] and [MP, $Fe^{2+}P$] (prepared by $Na_2S_2O_4$ reduction).

Table III. Extinction Coefficient Differences for [α(FeP), β(MP)] Hybrids

species	λ, nm[a]	Δε, mM^{-1} cm^{-1}
^{3}(MgP)–MgP	432	0[b]
	543	0[b]
	415	−80 (5)[c]
	475	20 (2)[c]
^{3}(ZnP)–ZnP	436	0[b]
	542	0[b]
	415	−80[d]
	475	20[d]
$Fe^{2+}P$–$Fe^{3+}(H_2O)P$	415	0[b]
	432	50 (2)
	436	41 (2)
$(MgP)^+$–MgP	432	−5 (2)[c]
$(ZnP)^+$–ZnP	436	−3 (2)[c]

[a] ±0.5 nm. [b] ±1%. [c] Calculated by using ϵ_{MgHb}(420 nm) = 150 000 M^{-1} cm^{-1} subunit^{-1}.[16] [d] Calculated by comparison to the $(ZnCcP)^+$–ZnCcP difference spectrum (see text).

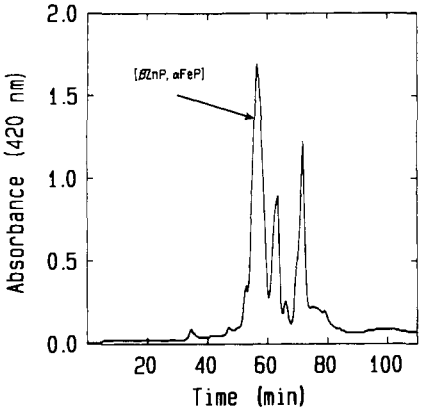

Figure 1. Typical HPLC chromatogram of the [β(ZnP), α(Fe^{2+}(CO)P)] hybrid. ~100 mg of reaction mixture was loaded onto a 21.5 mm × 15 cm Beckman SP-5PW ion-exchange column equilibrated with 25 mM KP_i, pH 6.0 (4 °C), and eluted with a 90-min linear gradient to 25 mM dibasic KP_i at a flow rate of 5 mL/min. The peak with a retention time corresponding to 56 min was pooled as hybrid.

The instability of $(MP)^+$ within a Hb subunit precludes direct measurement of the [$(MP)^+$Hb–MPHb] absorbance difference spectrum. The cation $(ZnP)^+$ is not sufficiently stable when incorporated into an Hb chain or Mb for static spectra to be taken. Therefore, we approximate $\Delta\epsilon((ZnP)^+$–ZnP) for the hybrid at its ^{3}(ZnP)/ZnP isosbestic points, 436 nm, with the value measured for Zn-substituted cytochrome c peroxidase at its Soret region triplet isosbestic point, 445 nm (Table III).[17] Extinction coefficient differences at the ^{3}(MP)/MP Soret isosbestic points, ϵ([$(MP)^+$, $Fe^{2+}P$]) – ϵ([MP, $Fe^{3+}(H_2O)P$]) ≡ ($\epsilon_1 - \epsilon_A$) and ϵ([MP, $Fe^{2+}P$]) – ϵ([MP, $Fe^{3+}P$]) ≡ ($\epsilon_C - \epsilon_A$), were calculated by using eq 4 and the data listed in Table III.

$$\epsilon_1 - \epsilon_A \approx \{\epsilon((MP)^+) - \epsilon(MP)\} + \{\epsilon(Fe^{2+}P) - \epsilon(Fe^{3+}(H_2O)P\} \quad (4a)$$

$$\epsilon_C - \epsilon_A = \epsilon(Fe^{2+}P) - \epsilon(Fe^{3+}(H_2O)P) \quad (4b)$$

Results

Preparation of MHb and Mixed-Metal Hb Hybrids. A typical preparative HPLC chromatogram of the [β(ZnP), α(Fe^{2+}(CO)P] hybrid is shown in Figure 1. The hybrid has a retention time of approximately 56 min and appears as a single band in an analytical IEF gel. The peak with retention time of ~72 min corresponds to excess α(Fe(CO)P) chains. Similar results are obtained for the [β(MgP), α(Fe^{2+}(CO)P] hybrid. As expected from the ligation difference, the retention time of ZnHb and MgHb in HPLC chromatograms with this buffer system, ~70 min (69 and 72 min, respectively), differs from that of the partially ligated hybrids.

Crystal Structure of MgHb. The X-ray diffraction measurements of MgHb show that it crystallizes in the same space group

(15) Bevington, P. R. *Data Reduction and Error Analysis for the Physical Sciences*; McGraw-Hill: New York, 1969.
(16) Coon, O. C.; Rodley, G. A. *J. Inorg. Biochem.* **1983**, *19*, 189–202.
(17) Liang, N.; Mauk, G. A.; Pielak, G. J.; Johnson, J. A.; Smith, M.; Hoffman, B. M. *Science* **1988**, *240*, 311–313.

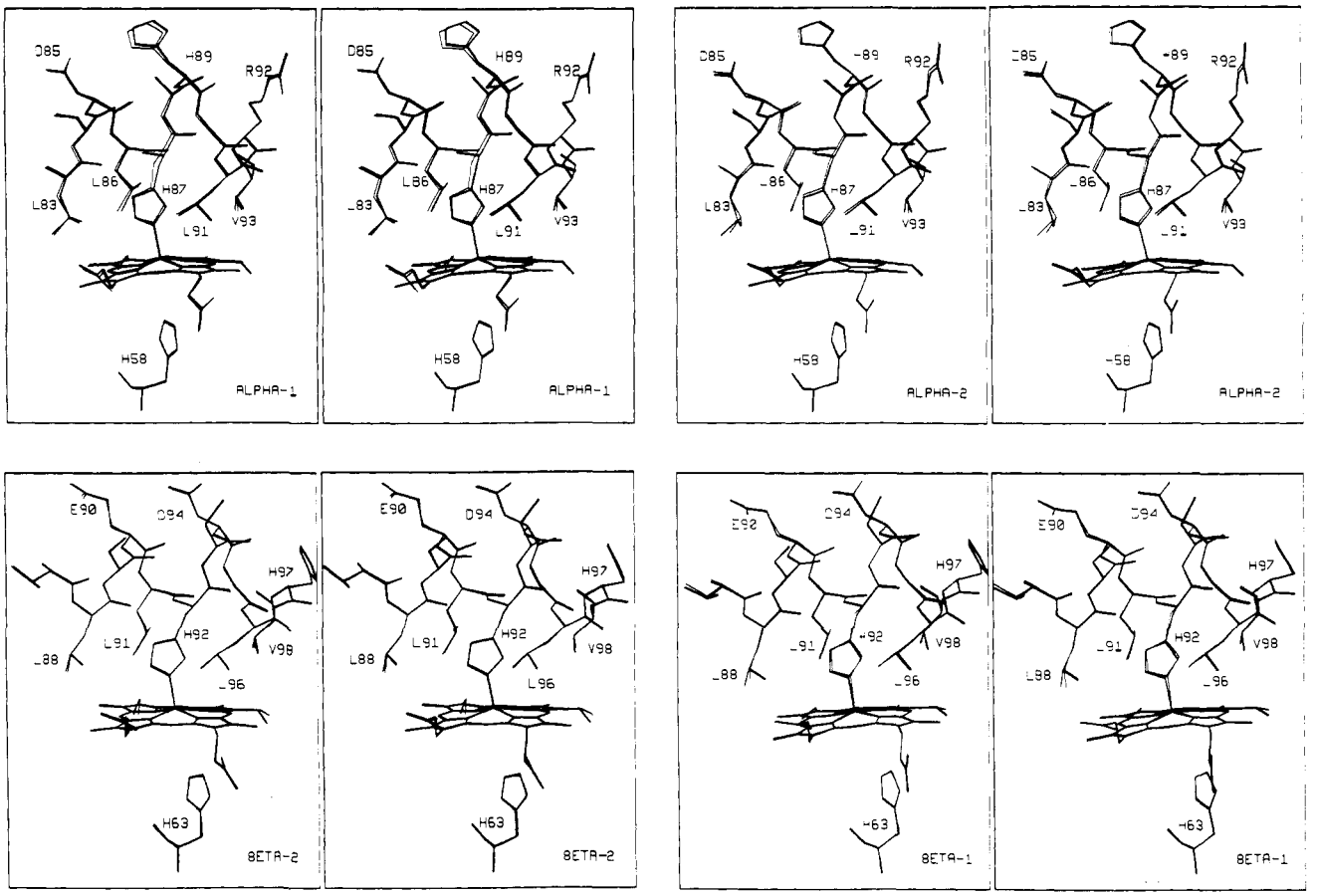

Figure 2. (A) Left: Superposition of MgHb and deoxyHb structures in the regions of the α_1 (upper) and β_2 (lower) heme pockets. (B) Right: Corresponding superpositions for the α_2 (upper) and β_1 (lower) heme pockets. The MgHb and deoxyHb structures are drawn with thin and thick lines, respectively.

and is isomorphous with deoxyFeHb. This gives direct structural evidence that Mg and Zn substitution favors the deoxy, or T, quaternary structure. Figure 2A shows a superposition of the MgHb and deoxyHb structures in the region of the α_1 and β_2 heme pockets. Figure 2B shows the same superposition in the region of the α_2 and β_1 heme pockets. A plot of backbone deviations from exact superposition is given in Figure 3. The largest differences occur in the α_1 chain where the α-carbon of the His 87 has shifted by 0.28 Å and the ϵ-nitrogen of the surface residue His 89 shifts by 0.46 Å. However, as movements of these magnitudes are not observed for the corresponding atoms in the α_2 chain, and as all the other backbone shifts are smaller in magnitude, we conclude that the substitution of Mg^{II} for Fe^{II} causes no significant perturbations that can be detected at the current resolution of our diffraction data. A 2.1-Å difference electron density map (generated with $\{[\alpha(Mg^{II})\beta(Mg^{II})]_2-[\alpha(Fe^{II})\beta(Fe^{II})]_2\}$ structure factors and calculated phases) shows only large peaks of negative density at the heme metal positions, as expected for the replacement of Fe (z = 26) by Mg (z = 12), confirming this conclusion.

Spectroscopic Properties. Optical spectra and a partial [^{3}(ZnP)–ZnP] difference spectrum for ZnHb have been presented previously.[14] Figure 4 shows the [^{3}(ZnP)–ZnP] transient difference spectrum in the region 380–600 nm. Noteworthy features include the strong negative feature at λ = 424 nm that corresponds to bleaching of the ZnP Soret band, the small positive absorbance difference at λ = 475 nm, and isosbestic points at λ = 436 and 542 nm (Table III). The transient difference spectra for ZnHb and [ZnP, Fe^{2+}P] are identical. The [^{3}(MgP)–MgP] transient difference spectrum obtained upon flash photolysis of MgHb or [MgHb, Fe^{2+}P] is quite similar (not shown); its principal isosbestic points also are given in Table III.

The static {[MP, Fe^{2+}P]–[MP, $Fe^{3+}(H_2O)$P]} difference spectrum is the same for M = Zn and Mg and is shown in Figure 5; the Fe^{3+}P/Fe^{2+}P isosbestic point is given in Table III. For reference, arrows in the figure refer to locations of ^{3}(MgP)/MgP isosbestic points. The figure shows that the absorbance changes associated with formation of Fe^{2+}P within I should be relatively large and positive at the Soret region ^{3}(MP)/MP isosbestic points but small and negative at those in the α/β region; the net extinction coefficient differences between I and A at ^{3}(MP)/MP isosbestic points are calculated by use of eq 4.

Triplet Decay of [^{3}(MP), Fe^{2+}P] and [^{3}(MP), $Fe^{3+}(H_2O)$P]. Photoexcitation of [MP, FeP] hybrids leads to production of the long-lived ^{3}(MP) triplet state. Figure 6 shows normalized decay curves for [^{3}(MP), $Fe^{3+}(H_2O)$P] and [^{3}(MP), Fe^{2+}P]; identical data are obtained when the triplet decay is monitored by transient absorbance (Figure 5) and by luminescence. In each case, triplet decay follows an exponential time course for at least 5 half-lives. For the Fe^{2+} hybrids the decay rate constants are k_D^{Mg} = 20 (3) s^{-1} and k_D^{Zn} = 55 (5) s^{-1}. Triplet quenching by ferriheme within [MP, $Fe^{3+}(H_2O)$P] increases the triplet-decay rate constants to $k_p^{Mg}(H_2O)$ = 50 (5) s^{-1} and $k_p^{Zn}(H_2O)$ = 135 (10) s^{-1}. We define the quenching rate constant for [MP, $Fe^{3+}(H_2O)$P] hybrids as $k_q^{M}(H_2O) = k_p^{M}(H_2O) - k_D^{M}$; $k_q^{Zn}(H_2O)$ = 80 (15) s^{-1}; k_q^{Mg} = 30 (8) s^{-1}. In the absence of energy transfer in either oxidation state, k_D equals the intrinsic triplet-state decay constant, k_i, the quenching within the oxidized hybrids represents ^{3}(MP) → $Fe^{3+}(H_2O)$P electron transfer, and $k_q = k_t$ (eq 1). However, in the presence of energy-transfer quenching in the [MP, Fe^{2+}P] hybrid (rate constant k_E^{2+}) and/or [MP, $Fe^{3+}(H_2O)$P] hybrid (rate constant $k_E^{3+}(H_2O)$), $k_D = k_i + k_E^{2+}$, $k_p = k_i + k_t + k_E^{3+}(H_2O)$, and $k_q = k_p - k_D = k_t + \Delta k_E$, where Δk_E is the difference between the energy-transfer rate constants of the oxidized and reduced forms. Direct observation of the charge-separated intermediate I (see below) verifies that the triplet quenching within [^{3}(MP), $Fe^{3+}(H_2O)$P] is primarily due to ^{3}(MP) → $Fe^{3+}(H_2O)$P electron transfer, namely $\Delta k_E \ll k_q$.

Observation of the Charge-Separated Intermediate I. Figure 7 shows the time course of the transient absorbance monitored

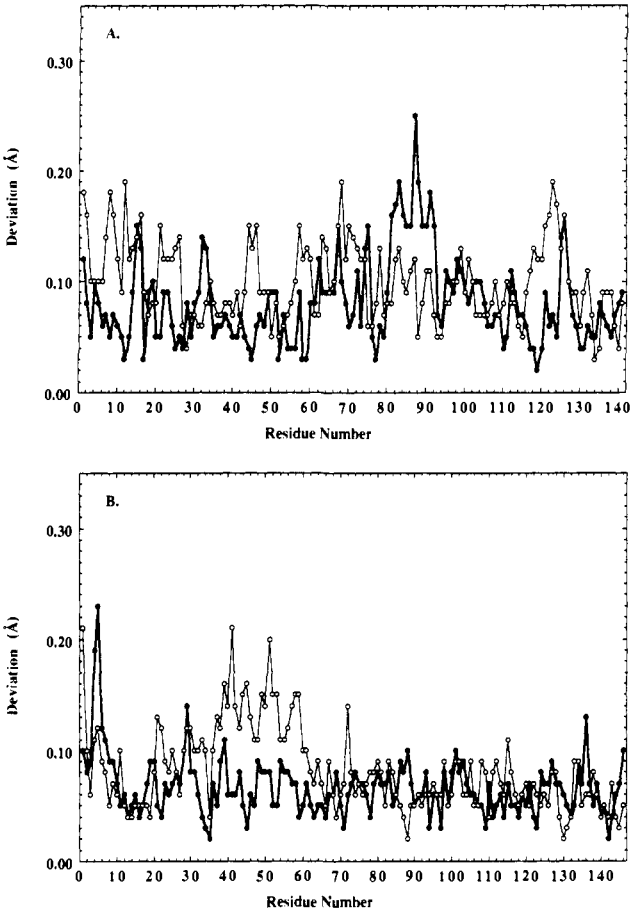

Figure 3. Deviations from exact superposition (averaged over the backbone atoms) of the deoxyFeHb versus MgHb atomic models. (A) The thick curve shows the α_1 subunit deviations; the thin curve, the α_2 subunit deviations. (B) Corresponding curves for the β_1 (thick line) and β_2 (thin line) subunit deviations.

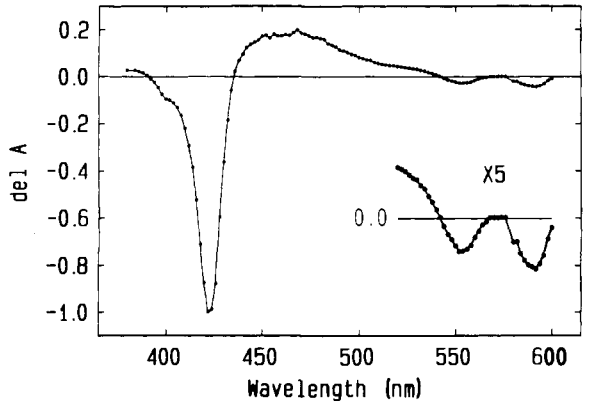

Figure 4. [^{3}(ZnP) − ZnP] kinetic difference spectrum of ZnHb. Conditions: 0.050 M KP_i, pH 7.0; [tetramer] ~ 3 μM; [IHP] ~ 25 μM.

at two ^{3}(MgP)/MgP isosbestic points (432 and 542 nm) following flash photolysis of [MgP, $Fe^{3+}(H_2O)P$] as well as a trace following flash excitation of [MgP, $Fe^{2+}P$]. For the Fe^{3+} hybrid, the absorbance of the transient at the λ = 432 nm ^{3}(MgP)/MgP isosbestic point is large and positive, whereas that at the 542-nm isosbestic point is small and negative. Identification of the kinetic transient with I is confirmed as follows: (i) The [MgP, $Fe^{2+}P$] hybrid shows no transient (Figure 7), and the magnitude of the transient is proportional to the concentration of $Fe^{3+}(H_2O)P$ in partially reduced samples (not shown). (ii) Not only are the signs of the kinetic absorbance changes at 432 and 542 nm as expected (Figure 7), but also the roughly 8-fold larger magnitude at 432 nm is consistent with the extinction coefficient differences (Table III) predicted for the formation of the charge-transfer intermediate, I, in accord with the kinetic scheme of eqs 1 and 2. (iii) As discussed below, the two progress curves for [MgP,

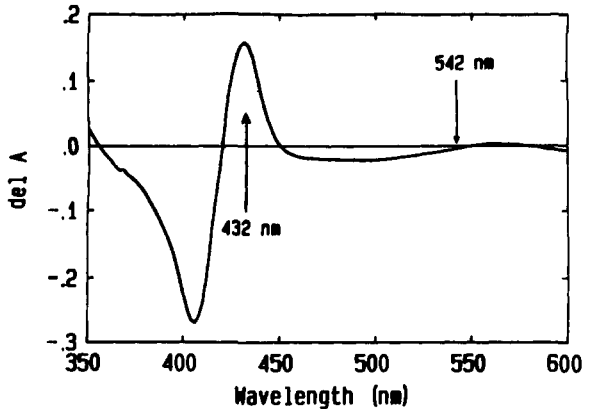

Figure 5. {[β(MgP), $\alpha(Fe^{2+}P)$]−[β(MgP), $\alpha(Fe^{3+}(H_2O)P)$]} optical difference spectrum. The reduced hybrid was prepared by reduction of oxidized hybrid (~5 μM) in 0.010 M KP_i, pH 7.00 (see text).

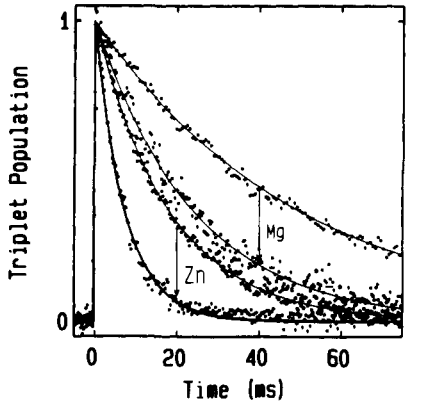

Figure 6. Normalized progress curves for the decay of A* subsequent to flash photolysis of [β(ZnP), $\alpha(Fe^{2+}P)$] and [β(MgP), $\alpha(Fe^{3+}(H_2O)P)$] Hb hybrids at 415 nm. Arrows go from traces for Fe^{2+} hybrid to those for Fe^{3+} hybrid. Solid curves are the nonlinear least-squares fit to eq 6 in text. Conditions: 0.01 M KP_i, pH 7.0; [IHP] = 25 μM; temperature = 25 °C; [tetramer] ~ 2 μM. Key: (a) [β(ZnP), $\alpha(Fe^{3+}(H_2O)P)$]; (b) [β(ZnP), $\alpha(Fe^{2+}P)$]; (c) [β(MgP), $\alpha(Fe^{3+}(H_2O)P)$]; (d) [β(MgP), $\alpha(Fe^{2+}P)$].

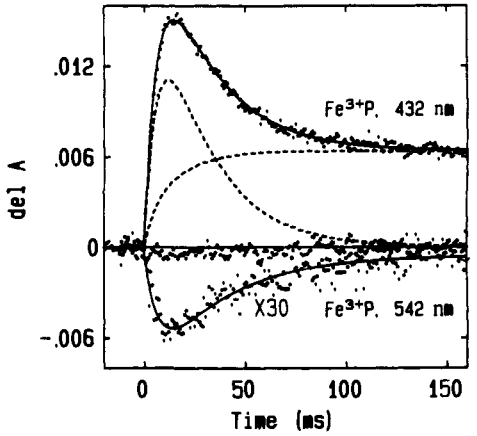

Figure 7. Kinetic progress curves obtained by photolysis of [β(MgP), $\alpha(Fe^{3+}(H_2O)P)$] (top and bottom traces) and [β(MgP), $\alpha(Fe^{2+}P)$] (center trace). The top data set is for [MgP, $Fe^{3+}(H_2O)P$] at λ = 432 nm. The solid line is the nonlinear least-squares fit with k_x = 155 (10) s^{-1}, k_p = 37 (5) s^{-1}, ΔA_∞ = 0.0064 (4), and β = 3.4 (3). The dashed lines are the decomposition of the fit into components for I and C. The bottom trace (and corresponding fit) was obtained with a different sample at λ = 542 nm [k_x = 155 (15) s^{-1}, k_p = 29 (8) s^{-1}, ΔA_∞ = −0.000 02 (1), and β = −0.05 (4)]. The center trace is the kinetic transient obtained with [MgP, $Fe^{2+}P$] at λ = 432 nm. An identical transient (not shown) was obtained with this hybrid at 542 nm. Conditions: 0.01 M KP_i, pH 7.0; [tetramer] ~ 2.5 μM; [IHP] = 25 μM.

$Fe^{3+}(H_2O)P$] (Figure 7) and those for [ZnP, $Fe^{3+}(H_2O)P$] (data not shown) are well-fit by the equations obtained from the kinetic scheme of eqs 1 and 2 when extended to accommodate the observation of a persistent change (ΔA_∞) at the ^{3}(MP)/MP isosbestic point; this indicates that $(MP)^+$ also is reduced by an unidentified amino acid X and/or solution impurities (eq 5), with a rate

$$\underset{\text{I}}{[(MP)^+, Fe^{2+}P]} + X \xrightarrow{k_m} \underset{\text{C}}{[MP, Fe^{2+}P]} + X^+ \qquad (5)$$

constant k_m. It is worth noting that the formation of C by itself constitutes unambiguous proof of photoinitiated electron transfer within mixed-metal hemoglobin hybrids.

Solution of the differential equations that describe the ET kinetic scheme (eqs 1, 2, and 5) gives the time-dependent concentrations $A^*(t)$, $I(t)$, and $C(t)$ shown in eqs 6–8, where A^*_0 is

$$A^*(t) = A^*_0 \exp(-k_p t) \qquad (6)$$

$$I(t) = k_1 A^*_0 \frac{\exp(-k_p t) - \exp(-k_x t)}{k_x - k_p} \equiv k_1 A^*_0 i(t) \qquad (7)$$

$$C(t) = \frac{k_m k_1 A^*_0}{k_x k_p} \frac{k_p(\exp(-k_x t) - 1) + k_x(1 - \exp(-k_p t))}{k_x - k_p} \equiv \frac{k_m k_1 A^*_0}{k_x k_p} c(t) \qquad (8)$$

the concentration of A* produced by the actinic flash at $t = 0$ and we define $k_x = k_b + k_m$. At a ^{3}(MP)/MP isosbestic point, the observed absorbance change, $\Delta A(t)$, is the sum of contributions from $I(t)$ and $C(t)$:

$$\Delta A(t) = \beta(i(t)) + (\Delta A_\infty)(c(t)) \qquad (9)$$

where

$$\Delta A_\infty = \frac{(\epsilon_C - \epsilon_A) k_m k_1 A^*_0}{k_x k_p} \qquad \beta = (\epsilon_I - \epsilon_A) k_1 A^*_0 \qquad (10)$$

At wavelengths other than an exact isosbestic, an exponential term of the form of eq 6 must be added to eq 9. When $k_x > k_p$, as is the case here, eq 9 predicts transient absorbance changes consisting of an exponential rise with rate constant k_x and an exponential fall with rate constant k_p to a persistent absorbance change, ΔA_∞, which is proportional to k_m (eq 10). The fact that I and A* disappear synchronously, with rate constant k_p, means at wavelengths other than near an A*/A isosbestic point, the absorbance change associated with I is swamped by that of A*. Furthermore, A* absorbs almost continuously from $\lambda > 380$ nm to $\lambda < 700$ nm, so there are no windows for observation of I other than near the A*/A isosbestic points.

As shown in the top trace of Figure 7, the transient absorbance changes caused by electron transfer are well-described by nonlinear least-squares fits to eq 9 that yield the parameters $k_x = 155$ (10) s^{-1}, $k_p = 37$ (5) s^{-1}, $\Delta A_\infty = 6.40$ (40) $\times 10^{-3}$, and $\beta = 3.4$ (3). Theoretical curves in this figure include the total absorbance change calculated with these parameters (eq 9) as well as a decomposition into the contributions from $I(t)$ and $C(t)$. Algebraic manipulation of the expressions for ΔA_∞ and β (eq 10) gives an expression for k_m (eq 11) where $P = (\epsilon_I - \epsilon_A)/(\epsilon_C - \epsilon_A)$ is calculated

$$k_m = \frac{k_x k_p (\Delta A_\infty) P}{\beta} \qquad (11)$$

with use of eq 4. This analysis yields $k_m = 10$ (5) s^{-1} and $k_b = 145$ (12) s^{-1}. Although the rate constant k_m is well-defined for an individual sample, it varies between samples and thus is likely to be associated in part with impurities. Thus, it is not discussed further.

Direct Determination of k_1. Although k_q determined by measuring triplet decay rates can have contributions from both electron and energy transfer, k_1 can be determined independently through use of eq 10. The quantity A^*_0 in eq 10 is determined from the zero-time absorbance change of the triplet state, as measured at 475 nm,[18] through use of the extinction coefficient difference, $\{\epsilon(^3(MP)) - \epsilon(MP)\}$ (Table III).[14] A typical experiment with the [ZnP, $Fe^{3+}(H_2O)P$] hybrid gives $k_1^{Zn} = 85$ (20) s^{-1}, which is comparable to the quenching rate measured by monitoring the decay of A*, $k_q^{Zn} = k_p^{Zn} - k_D^{Zn} = 74$ (5) s^{-1}. Thus, for this hybrid, $k_1^{Zn} \sim k_q^{Zn}$ and the triplet quenching is essentially an electron-transfer process, as originally inferred.[19a] We find the same is true for the Mg hybrid, with $k_1^{Mg} = 35$ (10) s^{-1}.

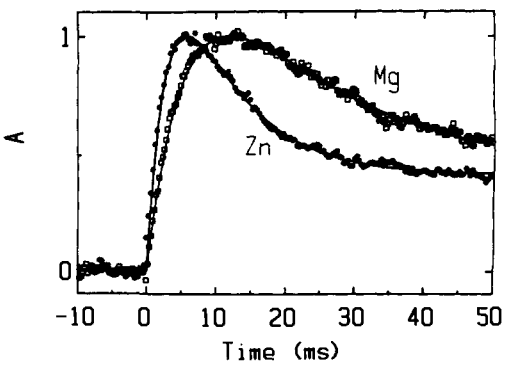

Figure 8. Normalized kinetic progress curves at 5 °C for Zn and Mg hybrids: [β(MgP), α($Fe^{3+}(H_2O)P$)] (λ = 432 nm); [β(ZnP), α($Fe^{3+}(H_2O)P$)] (λ = 436 nm). Solid lines are nonlinear least-squares fits to eq 9. For [Mg, Fe], $k_b = 155$ (15) s^{-1} and $k_m = 20$ (5) s^{-1}; for [Zn, Fe], $k_b = 350$ (35) s^{-1}, $k_p = 112$ (10) s^{-1}, and $k_m = 40$ (8) s^{-1}. Conditions: 0.01 M KP_i, pH 7.0; [tetramer] ~ 2.5 μM; [IHP] = 25 μM.

Table IV. Electron-Transfer Kinetic Parameters for [$\alpha(Fe^{3+}(H_2O)P$, β(MP)] Hybrids[a,b]

M	k_1(20 °C), s^{-1}	k_b(20 °C), s^{-1}	E_b, eV	E_1, eV
Zn	85 (15)	350 (35)	0.08 (1)	0.10 (2)
Mg	35 (8)	155 (15)	0.01 (3)	0.10 (3)

[a] Energies are Arrhenius activation parameters. [b] The rate parameters for eq 5 are k_m^{Zn}(20 °C) = 30 (8) s^{-1}, $E_m^{Zn} = 0.12$ (5) eV, k_m^{Mg}(20 °C) = 10 (5) s^{-1}, and $E_m^{Mg} = 0.31$ (5) eV.

Dependence of ET within [MP, $Fe^{3+}(H_2O)P$] on M and Temperature. Figure 8 superimposes normalized flash-photolysis kinetic progress curves (T = 278 K) for [MgP, $Fe^{3+}(H_2O)P$] and [ZnP, $Fe^{3+}(H_2O)P$] as monitored at their Soret region isosbestic points, along with nonlinear least-squares fits of the data to eq 9. The long-time decay in the transient absorbance is governed by k_p and is more rapid for M = Zn than for M = Mg (k_p^{Zn} = 112 s^{-1}, k_p^{Mg} = 47 s^{-1}), in agreement with the ^{3}(MP) decay traces presented in Figure 6. The rate constant, k_x, for the exponential rise also is larger for M = Zn than for M = Mg. Use of eq 11 shows that k_m^M is small and gives $k_b^{Zn} = 350$ s^{-1} and $k_b^{Mg} = 155$ s^{-1}. Thus, both the photoinitiated ^{3}(MP) → $Fe^{3+}(H_2O)P$ and thermal $Fe^{2+}P$ → $(MP)^+$ ET processes are more rapid for M = Zn.

The ET cycle (eqs 1, 2, and 5) has been studied from 0 to 25 °C for both [MP, FeP] hybrids, and Table IV shows the activation parameters obtained from Arrhenius plots for k_1, k_b, and k_m. Both k_1 and particularly k_b are essentially activationless.

Discussion

Our original studies of long-range ET in mixed-metal Hb hybrids used measurements of triplet quenching as evidence of ^{3}(ZnP) → $Fe^{3+}P$ electron transfer in the oxidized hybrid, and as a result, the rate constants for the $Fe^{2+}P$ → $(ZnP)^+$ process could not be measured.[19] Direct spectroscopic observation of the charge-separated intermediate, I, now confirms that the quenching within [MP, $Fe^{3+}(H_2O)P$] is in fact dominated by long-range ET. The time course of the kinetic transients is well-described by solutions to the kinetic equations for the ET processes in eqs 1,

(18) If the hybrid is not fully oxidized, then only the oxidized molecules are ET-active, and for calculation purposes, one decreases A^*_0 by the fraction of these molecules, g (see Experimental Section).

(19) (a) McGourty, J. L.; Peterson-Kennedy, S. E.; Ruo, W. Y.; Hoffman, B. M. *Biochemistry* **1987**, *26*, 8302–8312. (b) Peterson-Kennedy, S. E.; McGourty, J. L.; Kalweit, J. A.; Hoffman, B. M. *J. Am. Chem. Soc.* **1986**, *108*, 1739–1746.

2, and 5, and fits to eqs 6–8 have given the rate constant for the $Fe^{2+}P \rightarrow (MP)^+$ charge recombination.

Our choice of ZnP and MgP as photoactive substitutions for heme had been in part predicated on the similarity of their structures to that of the five-coordinate ferrous heme, as indicated by X-ray diffraction studies of model compounds.[20] Thus, we expected that these metals also would favor the deoxyHb(T) quaternary structure. This was supported by CO recombination studies with the [M,Fe] hybrids where M = Zn, Mg, and also Mn, which indicated that in each of these cases the bisligated hybrid [MP, Fe(CO)P] in solution can be quantitatively converted to the T state by the presence of IHP.[21] The present X-ray structure of MgHb confirms that the deoxyheme structure is unperturbed by substitution with Mg and, in combination with the CO-rebinding data, leaves no doubt that the electron-transfer rate constants reported here refer to the [α_2(FeP), β_2(MP)] hybrid in a completely defined T-state structure, as has been visualized in the X-ray structures of the [Mn^{II}P, Fe(CO)P] hybrids.[22] Thus, these rate constants become prime test cases for quantitative interpretation in terms of evolving theories of ET coupling through proteins.[23]

An apparent measurement of long-range electron transfer within or between protein complexes raises two important questions about the reaction mechanism.[24] First, are the ET processes single-step events, or do they involve a sequence of steps with one or more real intermediate states, such as one with an oxidized or reduced amino acid residue?[25] Second, does the rate constant indeed measure an ET event, or is ET "gated", namely, controlled by a slow conformational transformation to an electron-transfer-active state in which ET is rapid?[26]

It can be easily proved that the photoinitiated electron-transfer process described here (eq 1) is direct. An electron might hop indirectly from ^{3}(MP) to $Fe^{3+}P$, via oxidative triplet quenching by an amino acid, with subsequent reduction of $Fe^{3+}P$ by the amino acid anion. However, such oxidative quenching would also occur in the reduced (Fe^{2+}) hybrids because this process does not involve FeP. Thus, the increases in triplet quenching observed in the $Fe^{3+}P$ hybrids must be associated with a direct process.

Our data also indicate that the I → A electron-transfer process (eq 2) is direct. Consider the alternative, in which an amino acid, y, mediates electron flow from $Fe^{2+}P$ to $(MP)^+$ via the intermediate, [(MP), y^+, ($Fe^{2+}P$)], which decays by a second electron-transfer process back to the ground state. If the $(MP)^+ \rightarrow y$ reaction were rapid, and $Fe^{2+}P \rightarrow y^+$ electron transfer were rate limiting, then changing M[27] would not affect the observed rate constant, and k_b^{Mg} would equal k_b^{Zn}. In contrast, if $(MP)^+$ succeeded by rapid $Fe^{2+}P \rightarrow y^+$ ET, changing the heme ligand would not affect the ET rate. However, it has been shown recently that $k_b^{Mg}(H_2O) \neq k_b^{Zn}(H_2O) \neq k_b^{Zn}(CN^-)$.[4b] Therefore, we conclude that such a two-step electron-hopping mechanism is not applicable and that k_b describes direct $Fe^{2+}P \rightarrow (MP)^+$ electron transfer.

Comparison of rates for [M, Fe] hybrids where M = Mg and Zn tests whether electron transfer is "gated", i.e. controlled by a slow conformational transformation to an electron-transfer-active state, in which ET is presumed to be rapid. The rate of a conformational transformation would not change because of the alteration in driving force caused by the change from Zn to Mg.[27] As k_f and k_b are indeed different for the two M's, the processes observed here cannot represent a rate-limiting conformational interconversion.

One further feature of these measurements is that $k^{Zn}/k^{Mg} \sim 3$ for both ET processes, eqs 1 and 2. Our work on ligated hybrids[4b] and at low temperatures[30] suggests that this does not arise from differences in the nuclear factor due to driving-force differences. Thus, these results suggest that $|H_{AB}|^2$, the square of the matrix element describing the electronic coupling between the donor and acceptor metalloporphyrins, for Zn may be roughly double that for Mg. We can understand such small dependences on the metal ion if, for example, one assumes that the MO's of MgP differ sufficiently from those of ZnP so as to cause slightly different couplings between the porphyrin orbitals and those of globin residues of the heme pocket.

Acknowledgment. This research has been supported by NIH Grants HL 13531 (B.M.H.) and HL 40453 (B.M.H., A.A.), by NSF Grant DMB 8907559 (B.M.H.), and by NIH NRSA postdoctoral fellowship HL 07531 (M.J.N.). We thank Gregory Martin for the purification of Hb, its separation into α and β chains, and the preparation of MgHb. We also thank Professors H. B. Gray and D. N. Beratan for fruitful discussions.

(20) Scheidt, W. R.; Lee, Y. J. *Struct. Bonding (Berlin)* **1987**, *64*, 1–70.

(21) (a) Blough, N. V.; Zemel, H.; Hoffman, B. M.; Lee, T. C. K.; Gibson, Q. H. *J. Am. Chem. Soc.* **1980**, *102*, 5683–5685. (b) Natan, M. J.; Kuila, D. Unpublished observations. (c) Blough, N. V.; Hoffman, B. M. *J. Am. Chem. Soc.* **1982**, *104*, 4247–4250.

(22) (a) Arnone, A.; Rogers, P.; Blough, N. V.; McGourty, J. L.; Hoffman, B. M. *J. Mol. Biol.* **1986**, 693–700. (b) Arnone, A., et al. Manuscript in preparation. (c) Efforts to crystallize [Fe, Mg] Hb hybrids also are underway.

(23) Beratan, D. N.; Onuchic, J. N.; Betts, J.; Bowler, B. E.; Gray, H. B. *J. Am. Chem. Soc.* **1990**, *112*, 7915–7921.

(24) Natan, M. J.; Baxter, W. W.; Kuila, D.; Gingrich, D. J.; Martin, G.; Hoffman, B. M. *Electron Transfer in Inorganic, Organic, and Biological Systems*; ACS Symposium Series; American Chemical Society: Washington, DC, 1990, in press.

(25) DeFillipis, M. R.; Faraggi, M.; Kapper, M. H. *J. Am. Chem. Soc.* **1990**, *112*, 5640–5642.

(26) (a) Hoffman, B. M.; Ratner, M. A. *J. Am. Chem. Soc.* **1987**, *109*, 6237–6243. (b) Hoffman, B. M.; Ratner, M. A.; Wallin, S. A. In *Electron Transfer in Biology and the Solid State*; Johnson, M. K., King, R. B., Kurtz, D. M., Jr., Kutal, C., Norton, M. L., Scott, R. A., Eds.; Advances in Chemistry Series 226; American Chemical Society: Washington, DC, 1990; pp 125–146. (c) Hazzard, J. T.; McLendon, G.; Cusanovich, M. A.; Tollin, G. *Biochem. Biophys. Res. Commun.* **1988**, *151*, 429–432.

(27) The $(MgP)^+/MgP$ reduction potential is about 100 mV lower than the $(ZnP)^+/ZnP$ reduction potential.[28,29] Consequently, $-\Delta G$ for the photoinitiated A* → I process is 1.0 eV for [^{3}(ZnP), $Fe^{3+}P$] and 1.1 eV for [^{3}MgP), $Fe^{3+}P$], while, for the I → A ET, $-\Delta G$ is 0.8 eV for [$(ZnP)^+$, $Fe^{2+}P$] and 0.7 eV for [$(MgP)^+$, $Fe^{2+}P$].

(28) (a) Stanienda, A. *Z. Naturforsch., B* **1978**, *23*, 147–152. (b) Felton, R. H. In *The Porphyrins*; Dolphin, D., Ed.; Academic: New York, 1986; Vol. 5, pp 53–125. (c) Davis, D. G. In *The Porphyrins*; Dolphin, D., Ed.; Academic: New York, 1986; Vol. 5, pp 127–151.

(29) (a) Deguchi, J.; Tamura, M.; Yamazaki, I. *J. Biol. Chem.* **1982**, *257*, 11517–11522. (b) Kaneko, Y.; Tamura, M.; Yamazaki, I. *Biochemistry* **1980**, *19*, 5795–5799.

(30) Kuila, D.; Baxter, W. W.; Natan, M. J.; Hoffman, B. M. *J. Phys. Chem.* **1991**, *95*, 1–3.